Available online at www.sciencedirect.com
ScienceDirect
Geomorphology 97 (2008) 5–23
GEOMORPHOLOGY
www.elsevier.com/locate/geomorph

Quantifying periglacial erosion in the Nepal high Himalaya

Arjun M. Heimsath [b,*], Robert McGlynn [a]

[a] Department of Earth Sciences, 6105 Fairchild Hall, Dartmouth College, Hanover, NH 03755, United States
[b] School of Earth and Space Exploration, Arizona State University, Tempe, AZ 85287, USA

Received 2 October 2006; received in revised form 28 November 2006; accepted 22 February 2007
Available online 23 June 2007

Abstract

Quantifying erosion rates in high mountain environments is challenging because the erosional processes are often stochastic and catastrophic. Distinguishing between periglacial and glacial rates is especially challenging. In this study we focus on determining erosion rates from a glaciated alpine landscape where the bedrock sidewalls are eroding predominantly by blockfall. We utilize a topographically well-constrained, debris-covered glacier on the north slope of the Annapurna Range, central Nepal Himalaya, to quantify an average headwall retreat rate. By measuring supraglacial debris depths from 0.1 to 2.4 m and average short-term down-valley transport rates of 17 m/yr we calculate a yearly sediment flux of 5820±1990 m^3/yr. The supraglacial debris originates from the steep, rocky headwall of the valley and we use the calculated flux with an estimated headwall contributing area to determine a slope-perpendicular headwall retreat rate of 1.3±0.5 mm/yr, which corresponds to a vertical lowering rate of 0.42±0.16 mm/yr and a horizontal retreat rate of 1.2±0.5 mm/yr. This rate is significantly greater than the steady-state erosion rates that we determine for the valley ridge crests and sidewalls (0.08±0.03 mm/yr and 0.20±0.05 mm/yr, respectively) using concentrations of the in situ produced cosmogenic radionuclide, ^{10}Be. Additionally, ^{10}Be exposure ages of the lateral moraine crests and supraglacial debris suggest a glacial advance about 470 yr ago and a long-term supraglacial transport rate of about 10 m/yr. Using this long-term transport rate reduces our inferred headwall retreat and suggests that the up-glacial bedrock slopes are eroding at roughly the same rate. While our results do not quantify the rate of glacial erosion, the absence of a glacial gorge suggests that there may be a rough balance between glacial downcutting and the erosion of the valley sidewalls. Rates quantified here are almost an order of magnitude lower than fluvial incision rates of the upper Marsyandi River that drains the study area, suggesting that even glaciated catchments are not keeping pace with the rapidly down-cutting rivers of the Himalaya.

Keywords: ^{10}Be; Cosmogenic nuclides; Supraglacial debris; Marsyandi River; Headwall retreat

1. Introduction

Topographic evolution in mountain ranges results from the interplay between tectonic forcing of the crust, erosional processes acting on the landscape, and any isostatic response of the range to erosion. For a given tectonic forcing, the evolution of the range, and the associated sediment delivery from the range, will depend on the rates and processes of erosion. While glaciers are widely thought to be the most effective erosional agents (e.g. Hallet et al., 1996; Brozovic et al., 1997; Montgomery, 2002), it is likely that periglacial processes eroding the typically bedrock-dominated slopes above the glaciers play a critical role in eroding the landscape (e.g. André, 1997; Zhang et al., 2001; Pan et al., 2003). In this study we focus on the periglacial processes contributing sediment to a glaciated landscape.

For any mountain range, the relative rates of tectonic and climatic forcing, with their associated cycles, set the

* Corresponding author.
E-mail address: Arjun.Heimsath@asu.edu (A.M. Heimsath).

0169-555X/$ - see front matter © 2007 Elsevier B.V. All rights reserved.
doi:10.1016/j.geomorph.2007.02.046

pace of how the landscape evolves as well as the morphology of the range. For the Himalaya, the dramatically high relief is thought to result from high erosion rates due to the onset of glacial cycles in combination with extremely high rates of tectonic uplift (e.g. Shroder and Bishop, 2000; Zeitler et al., 2001). A debate exists on the relative roles of climatic and tectonic forces on mountain building, as well as on the potential linkages between late Cenozoic uplift of the Tibetan Plateau and the onset of Quaternary glaciations (e.g. Molnar and England, 1990). Central to this debate, is quantifying the relative roles of different surficial processes (e.g. Burbank et al., 1996; Brozovic et al., 1997; Whipple and Tucker, 1999) and, specifically, the relative roles of glacial and fluvial erosion in creating relief (Harbor and Warburton, 1992, 1993; Whipple et al., 1999; Whipple and Tucker, 1999; Brocklehurst and Whipple, 2002; Montgomery, 2002). In a glaciated landscape, relief might increase, for example, if subglacial erosion rates are greater than fluvial incision rates (e.g. Hallet et al., 1996; Small and Anderson, 1998) while the ridge crests and valley sidewalls continue to erode more slowly.

In these high mountain environments, where vegetation is sparse and freeze–thaw cycles are common, blockfall is an important geomorphic process (e.g. Whalley, 1984; Shroder et al., 1999) and an important component of the overall erosion rate (Rapp, 1960; Barsch and Jakob, 1998; Matsuoka and Sakai, 1999). Steep bedrock cliffs suggest, for example, that blockfall is likely to be an important process controlling ridge crest lowering and headwall retreat (André, 1997). Such bedrock-dominated landscapes are not unique to glaciated regions and either glaciers or rivers must ultimately remove sediment delivered by blockfall. Relative contributions of erosion due to blockfall should, therefore, be incorporated into estimates of basin wide erosion rates inferred from other methods. Specifically, in glaciated basins where erosion rates have been quantified the relative role of periglacial processes is often unknown. For the purposes of this paper, we focus on the sediment produced by periglacial processes such as blockfall rather than the mechanisms driving the processes.

In this paper we quantify periglacial erosion and headwall retreat rates using a small, topographically constrained, debris-covered glacier by determining the flux of supraglacial debris being transported downslope by the glacier. We equate this flux with blockfall erosion of the headwall that contributes the debris mantling the glacier by making a first-order steady-state assumption that the glacier is acting like a conveyor belt removing debris derived from the headwall. We compare our inferred headwall retreat rate with erosion rates for ridge crests and valley sidewalls determined with concentrations of in situ produced cosmogenic ^{10}Be. Our study area is a small glacial valley on the north face of the Annapurna massif in the high Himalaya of central Nepal.

Studies quantifying erosion of the Himalaya have focused on varying spatial, (from sub-catchment to subcontinent) and temporal (from years to millennial) scales and yielded large ranges in erosion rates. For example, suspended sediment yields in proglacial streams have led to physical erosion rates ranging from 0.11 mm/yr–0.46 mm/yr for the Nubra basin in the Western Karakoram (Bhutiyani, 2000) to 3.45–4.21 mm/yr for the Batura Glacier in the Karakoram (Collins, 1998). Estimates of erosion rates from suspended sediments from the much larger drainage areas of the Ganges River varied from 0.6–1.0 mm/yr (Milliman and Syvitski, 1992; Summerfield and Hulton, 1994; Galy and France-Lanord, 2001). These studies fail, however, to distinguish between eroded material that is stored within valleys or beneath a glacier and freshly eroded sediment. Inferring erosion rates from suspended sediment in a glacial system has additional complexities. The mining of stored sediment beneath a glacier may not be representative of current rates, and can include glacial as well as non-glacial erosion processes. Many studies using suspended sediment analyses (e.g. Collins, 1978) have also shown that there are large seasonal and yearly fluctuations in sediment loads, suggesting that long records of suspended sediment concentrations are necessary to even hint at representative rates.

Cosmogenic nuclides concentrations in stream sediments can be used to infer basin-averaged erosion rates, although the methodology cannot resolve exposure histories of sediment derived from glaciated basins. For example, in several unglaciated catchments of the Lesser Himalaya, Nepal, Wobus et al. (2005) use cosmogenic ^{10}Be from sediments to determine average erosion rates ranging from about 0.2 to about 0.8 mm/yr, where the variation is inferred to be due to active thrusting. Vance et al. (2003) determined average erosion rates varying from 0.8 to 2.7 mm/yr for the Upper Ganges River, India using concentrations of cosmogenic ^{10}Be and ^{26}Al in stream sediments, where the variation correlated well with long-term exhumation rates determined from fission track analyses. They do not, however, attempt to distinguish glacial erosion from other processes.

Cosmogenic nuclides (^{10}Be and ^{26}Al) have also been used to date abandoned strath terraces to determine fluvial incision rates by dividing the terrace elevation

above the river by the terrace exposure age. Leland et al. (1998) determined rapid incision rates varying from 1 to 3 mm/yr to 9 to 12 mm/yr in the Indus River in northern Pakistan, and also suggested a correlation with differential exhumation rates. Pratt et al. (2002) and Pratt-Sitaula et al. (2004) also used strath terrace ages determined by cosmogenic nuclide dating to infer processes of episodic incision in the Marsyandi River, Nepal, with rates of about 1.5 mm/yr in the Lesser Himalaya to about 8.5 mm/yr in the Greater Himalaya. Suspended sediment flux can be used to infer short-term basin wide erosion rates while cosmogenic nuclide dating of strath terraces can be used to infer long-term fluvial incision rates. Neither of these methods, however, provides insight into the relative importance of different erosional processes acting across the landscape.

In the Nepal Himalaya, the presence of debris covered and rock glaciers suggest that blockfall is likely to be an important component of the overall erosion rate of the landscape (e.g. Fujii and Higuchi, 1977). Similarly, across the Himalaya, debris mantling of the ablation area of glaciers is common (e.g. Moribayashi, 1974; Moribayashi and Higuchi, 1977; Fujii and Higuchi, 1977; Benn and Lehmkuhl, 2000; Owen et al., 2003) and the sediment budget of debris-covered glaciers may be dominated by the transport of supraglacial material originating through rockfall (e.g. Small, 1987a,b; Benn and Evans, 1998; Owen et al., 2003). While such studies highlight the importance of blockfall, there are few field-based data quantifying headwall retreat rates, or even glacial erosion rates for such landscapes (note also the papers referenced in Nakawo et al., 2000).

2. Conceptual framework

Quantifying rockfall rates and cliff retreat rates is typically done in two ways. Eroded debris can be collected and volumes measured using natural (e.g. Rapp, 1960; Ono and Watanabe, 1986; Matsuoka and Sakai, 1999) and artificial (e.g. Church et al., 1979; Douglas, 1980) traps. If time since deposition began and the contributing area that the debris originated from are known, then the erosion rate can be quantified by dividing the volume deposited by the time and the contributing area. Matsuoka and Sakai (1999), for example, collected rockfall debris that had fallen onto a talus slope covered in snow during thawing periods in the Japanese Alps and determined a retreat rate of 0.01 mm/yr for the headwall of an abandoned cirque. Other studies estimated debris volumes within active rock glaciers of known age and inferred rockfall and headwall retreat rates (e.g. Wahrhaftig and Cox, 1959; Caine, 1974; Barsch, 1977b; Humlum, 2000).

Blockfall in alpine areas tends to occur due to freeze–thaw cycles acting along planes of weakness or fractures, leaving rock subject to failure and removal by mass wasting processes (e.g. Church et al., 1979; Walder and Hallet, 1986; Matsuoka, 1990, 1991). Irrespective of the processes causing the erosion of rocky slopes, in glaciated valleys blockfall from slopes adjacent to the glacier deposit debris upon the ice surface. This debris is then transported and deposited down valley at rates dependent on the flow of the glacier. Depending on the size and flow characteristics of the glacier, the sediments are transported in different proportions between supraglacial and englacial debris. If both the source area and the transported volumes of the sediment can be measured, then a blockfall erosion rate can be determined. Specifically, debris derived from the eroding headwall must be deposited upon the surface of a glacier that is actively transporting the sediment downslope. Assuming that the input rate of sediment from the headwall is the only source of sediment and is equal to the output rate (a first-order assumption), then the measured flux divided by the surface contributing area yields the slope-perpendicular retreat rate of the slope contributing the sediment. The equivalent vertical lowering rate is the slope-perpendicular rate times the cosine of the average headwall slope, while the horizontal retreat rate of the headwall is the slope-perpendicular rate times the sine of the average slope.

We write the mass balance equation for the amount of headwall erosion (E_{HW}) as being equal to the divergence of this sediment transport flux ($\nabla \cdot \widetilde{Q}_s$) per unit width away from the headwall:

$$E_{\mathrm{HW}} = \rho_r \frac{dh}{dt} = -\rho_s \nabla \cdot \widetilde{Q}_s \tag{1}$$

where ρ_r is the bulk density of intact rock, ρ_s is the bulk density of the supraglacial debris and $\mathrm{d}h/\mathrm{d}t$ is the horizontal retreat rate of the headwall. Solving this equation for $\mathrm{d}h/\mathrm{d}t$ suggests that quantifying the sediment transport flux of debris derived from the headwall will yield the headwall retreat rate if the respective bulk densities can be measured or estimated.

The sediment transport flux of the sediment transported on top of a glacier can be determined by measuring the debris depth and the downslope transport velocity of the sediment. For a given cross section across the glacier, flux of supraglacial debris is the cross-sectional area of debris (width times depth) multiplied by the downslope velocity. Flux of englacial

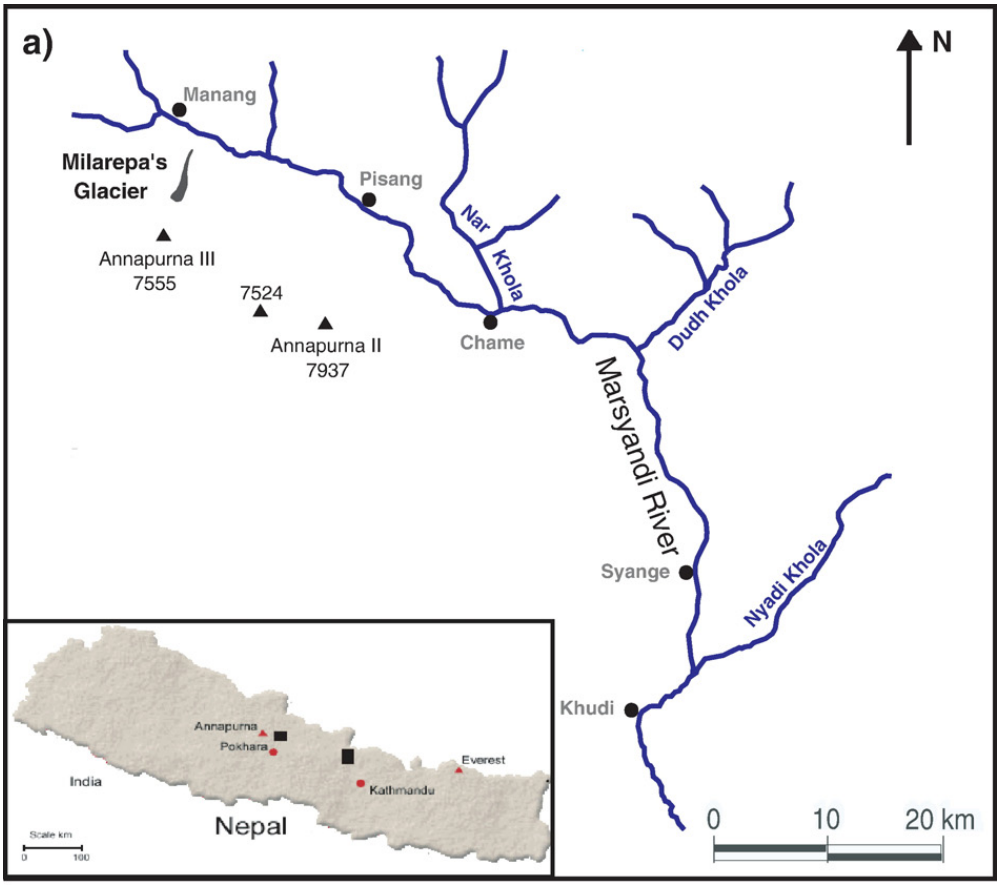

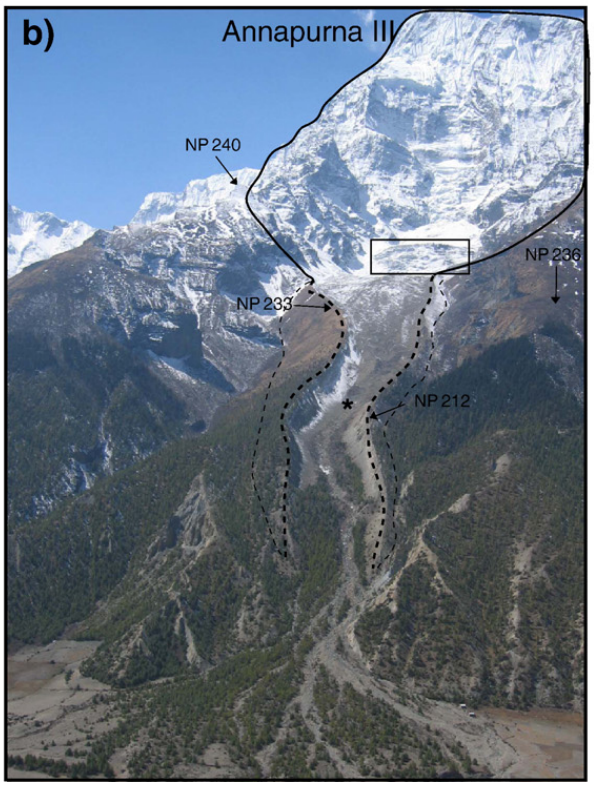

debris is the concentration of debris carried in the ice times the cross-sectional area of the ice times the velocity. Determining englacial sediment concentrations is an outstanding problem in glacial geomorphology and we use end-member estimates to constrain the potential range of sediment transported within the ice. Downslope velocity over short timescales can be determined by monitoring stable points on the surface of the glacier. Over long timescales, if the glacier surface is indeed acting like a conveyor belt transporting deposited debris away from the headwall, and if deposition ages can be determined for the deposited blocks, then downslope transport velocity is the distance of the block from the headwall divided by the deposition time.

2.1. Cosmogenic nuclides and bedrock erosion

While erosion due to blockfall represents a process occurring intermittently, bedrock landscapes are also eroding by continuous, grain-by-grain spallation or thin exfoliation sheet processes. Because these processes erode relatively thin layers of rock over relatively short time intervals they can be thought of as steady-state processes. Rates of such processes can be determined by collecting the thin outer layers of rock samples and measuring concentration of in situ produced ^{10}Be ($t_{1/2}=1.5\times10^6$ yr) and ^{26}Al ($t_{1/2}=0.7\times10^6$ yr) in the target mineral quartz (e.g. Nishiizumi et al., 1986, 1991; Lal, 1991; Gosse and Phillips, 2001). Comparing rates of erosion determined using cosmogenic nuclide concentrations to rates determined for block failure processes can help distinguish the relative efficacy of the different processes acting across a landscape.

Cosmogenic nuclide production rates on the Earth's surface decrease exponentially with depth in the target material such that the production rate, P (atoms/g yr), at some depth, $\times$ (cm), is (Lal, 1988):

$$P(x) = P(0)e^{-\rho x/\Lambda}, \tag{2}$$

where $P(0)$ is the surface production rate, ρ is the density of the target material (g/cm^3), and Λ is the absorption mean free path ($\sim$165 g/cm^2). The production rate of ^{10}Be has been determined experimentally and is found to be a function of altitude (increasing with altitude as atmospheric shielding mass decreases), latitude (increases from 0° to 50° N then stays roughly constant as the Earth's magnetic field changes — see Gosse and Phillips, 2001 for a thorough review), the geometry of exposure (topographic shielding of cosmic rays), and the density and composition of the target material (e.g. Lal, 1991, Nishiizumi et al., 1991). Nuclide concentration, N_s, at the rock surface is controlled by the nuclide production rate, the decay of the nuclide concentration, the steady-state erosion rate, ε, and time of exposure, t, such that for a steady-state exposure history,

$$N_s = \frac{P(0)}{\lambda+\mu\varepsilon}\left(1-e^{-(\lambda+\varepsilon\mu)t}\right), \tag{3}$$

where N_s is the nuclide concentration at the surface, λ is the disintegration constant ($\ln2/t_{1/2}$), μ is the absorption coefficient (ρ/Λ, cm^{-1}). Assuming that the surface has been eroding for a long enough time, such that a steady state or secular equilibrium has been reached, where $t \gg 1/(\lambda+\mu\varepsilon)$, Eq. (3) can be re-written as:

$$N_s = \frac{P(0)}{\lambda+\mu\varepsilon}, \tag{4}$$

or,

$$\frac{N_s}{P(0)} = \frac{1}{\lambda+\mu\varepsilon} = T_{\text{eff}}, \tag{5}$$

where T_{eff} is the effective exposure age (Lal, 1991). By rearranging Eq. (4) to solve for ε, the long-term erosion rate,

$$\varepsilon = \frac{1}{\mu}\left(\frac{P(0)}{N_s}-\lambda\right), \tag{6}$$

which is the equation commonly used to determine erosion rates from nuclide concentrations measured in bedrock samples (e.g. Lal, 1991; Nishiizumi et al., 1991; Small et al., 1997).

Fig. 1. (a) The study area along the Marsyandi River, central Nepal, with the overview map showing political boundary of Nepal inset into the lower left corner. The location of Milarepa's Glacier is north of Annapurna III and is denoted approximately by the rough shape (*J*).The glacier ranges in elevation from 3700–5350 m asl. (b) Photograph of the north face of Annapurna III taken from about 4500 m asl on the slope north of the Marsyandi River, which flows from right to left just out of view at the bottom of the photograph. Heavy dashed lines represent moraine crests with the upper elevation limit of the moraines being interpreted as the ELA. Lighter dashed lines show the approximate bottom of the lateral moraines, solid line encircles contributing area of sediment from the catchment headwall to the glacier surface, and the star denotes the terminus of the present day glacier. Note that the lateral moraines would block any potential contribution of sediment to the glacier surface from the valley sidewalls. The open black box encircles the low gradient, upper portion of the glacier that is mostly out of view in the photograph. Approximate locations of representative cosmogenic nuclide sample locations labeled as NP 212, 233, 236, and 240.

2.2. Exposure age dating

In environments lacking suitable organic matter for ^{14}C dating of glacial moraines, the cosmogenic nuclides ^{10}Be and ^{26}Al have been applied to determine glacial chronologies (e.g. Sloan and Phillips, 1998; Bierman et al., 1999; Phillips et al., 2000; Benn and Owen, 2002; Owen et al., 2002). Eq. (5) can be used to determine the minimum exposure age of moraines, or any surface, assuming no prior exposure of the sampled material, no post depositional erosion of the surface sampled, or exhumation of the surface by erosion. The reality in applying this methodology is that some samples do have inheritance of nuclide concentrations and that some erosion of the moraine surface occurs. Putkonen and Swanson (2003) suggest, for example, that cosmogenic dating of moraines requires numerous samples to discern the actual age of the moraine and propose a model for interpreting nuclide exposure ages.

Similarly, Eq. (5) can be used to date exposure ages of boulders, or aggregates of sediment deposited on the surface of the glacier. If these samples had no previous exposure to cosmogenic nuclide production, experienced no change in exposure geometry since being deposited on the glacier surface, and did not erode significantly during transport upon the glacier, then measured nuclide concentrations should increase systematically with distance from the sediment source area if the sediment transport rate was constant. Naturally, fulfilling all of these exposure constraints is unlikely for the active surface of a debris-mantled glacier, but we apply both of these dating applications to a small, debris-mantled glacier in the Nepal Himalaya.

3. Field site and methods

Our field area fits within the larger context of a trans-Himalayan transect used in several recent studies quantifying the connections between erosion, climate, and tectonic forcing (Pratt et al., 2002; Brewer et al., 2003; Burbank et al., 2003; Gabet et al., 2004a,b, Hodges et al., 2004; Pratt-Sitaula et al., 2004). Our study

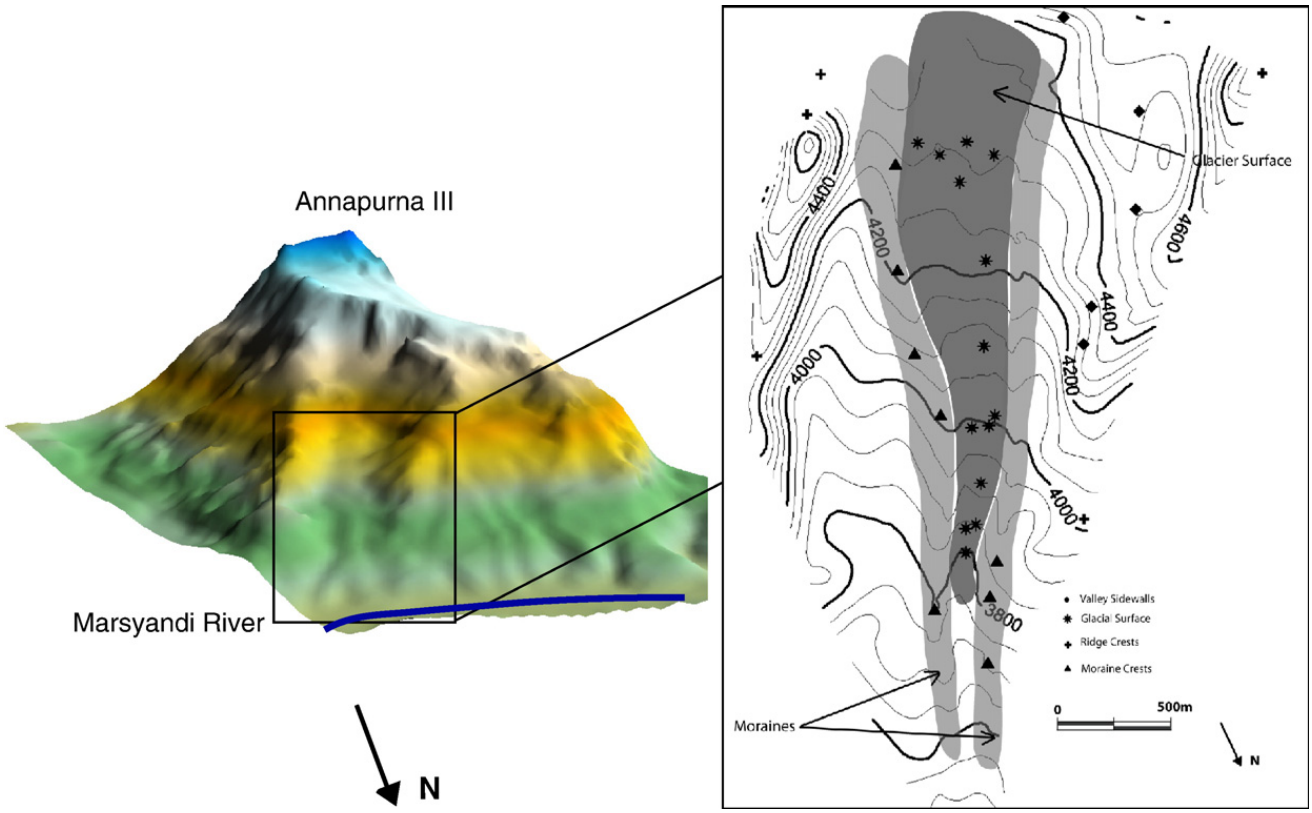

Fig. 2. DEM false-color image of the field site showing Annapurna III, Marsyandi River, and location of study area. Inset topographic map is from field surveying using a Trimble GPS RTK Total Station® 4700 showing locations of cosmogenic nuclide samples. Contour interval is 50 m. Valley sidewall sample locations are denoted by black diamonds, glacier surface sample locations shown with stars, ridge crest sample locations shown by black crosses and the moraine crest sample locations are shown by filled triangles. Headwall topography was determined from combining the DEM and the 1:50,000 topographic map (Nepal, 2001), but is omitted from the inset map for clarity. Inset map shows approximate boundaries of the two lateral moraines (light grey shading) as well as the present ice surface (dark grey shading), although the surveyed area did not extend into the accumulation area above 4400 m asl in elevation.

was designed to determine erosion rates upslope of the Marsyandi River in central Nepal and selected specifically because of the topographic constraints on a small, alpine glacier. The site, which we named Milarepa's Glacier because of the presence of a cave where the late 11th to early 12th Century Tibetan Buddhist Saint Milarepa meditated, is a small, debris-covered glacier, draining the north slope of Annapurna III into the Marsyandi River (Fig. 1, though the peak is out of view in the photograph, Fig. 1b).

3.1. Milarepa's glacier

Maximum relief of the steep (gradient of 1.4) bedrock headwall contributing to the glacier is 2200 m, rising from an elevation of 4400 m asl (where the dashed line on the crest of the left lateral moraine joins the solid black line outlining the basin in Fig. 1b) to 6600 m asl, the elevation of the top ridgeline. Most of the headwall area is the bowl-shaped area directly above the rectangle outlined on Fig. 1b, with distinct, small patches of ice frozen to it in various places. In other places, bedrock is clearly visible and is eroding by blockfall as well as ice-plucking. Block sizes evident on the surface of the glacier, and observed in avalanche deposits above the bergschrund, range from greater than 1 m^3 to cobble-sized clasts supported by a sandy-gravelly matrix. The main, bowl-shaped headwall map area, estimated from a high resolution topographic map (Nepal, 2001), is about 1.3 km^2, but because of it steep slope and bowl shape, its surface area contributing debris to the upper region of the accumulation area is about 4.5 km^2, estimated by breaking the topographic map into rectangles capturing roughly planar sections of the headwall. If the side slopes are included in this area calculation, they add another 1.7 km^2 in map area, or another 2.6 km^2 in contributing surface area. Their relative contribution to the debris mantling the glacier is uncertain, however, as the extensive avalanche and blockfall deposits at the base of the main bowl were not evident where these side slopes reached the accumulation area of the glacier. Side slopes down-valley from the contributing area outlined on Fig. 1b do not contribute sediment to the glacier surface due to the intervening ridges of the lateral moraines. All debris eroded from these slopes are forming talus slopes that can be seen on either side of the lightly dashed lines designating the base of each lateral moraine (Fig. 1b).

The upper limit of the lateral moraines suggests an equilibrium line altitude of 4350 m asl (Fig. 2), above which the accumulation area is a relatively small and steep region (gradient of almost 0.6, area of about 0.55 km^2) fed by avalanches and rockfall from the headwall. The top of the accumulation area is at an elevation of 5350 m asl and is marked by avalanche and blockfall deposits and an irregular, arcuit bergschrund. As evident in Fig. 1b, no debris deposition from the sidewalls was observed on the surface of the glacier downslope of the upper extent of the moraines – the moraines effectively shield the glacier from the side slopes downhill of the black rectangle drawn in Fig. 1b. The current ablation area is constrained between the two lateral moraines (Figs. 2 and 3) and narrows from almost 700 m in width at the broad, low gradient area at the

Fig. 3. Photograph of the view down-valley from the terminus of Milarepa's glacier showing the relatively un-dissected left lateral moraine (A) and right lateral moraine (B), with relief of about 40 m. Note that the Marsyandi River is visible in the valley bottom, roughly 2 km away. Scar on distant hillslope is a footpath.

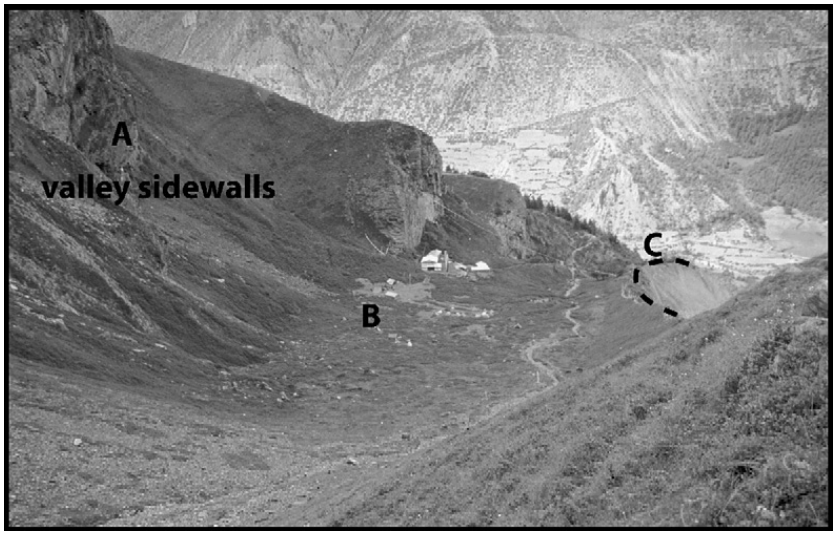

Fig. 4. Photograph of the valley west of the glacier. The valley sidewalls (A) are separated from surface of the glacier (off the right side of the photo) by a wide valley bottom (B) and the ridge formed by the left lateral moraine (uphill from pt. A in Fig. 3) shown by the dashed line on moraine crest (C). Structure in the middle of the photograph is a small monastery associated with Milarepa's cave.

uppermost extent of the lateral moraines, to 40 m in width at the terminus, marked by the star on Fig. 1b, at an elevation of 3700 m asl. The area of the ablation area is about 0.4 km^2, such that the ratio of the accumulation area to the total area of the glacier (AAR) is about 0.6, within the expected range of AARs for steady-state mountain glaciers (e.g. see review in Benn and Lehmkuhl, 2000), but much greater than the accumulation area observed on other debris-covered glaciers (e.g. Clark et al., 1994).

No prior work has been done on this glacier. The bedrock is part of the Tibetan Sedimentary Sequence, which is mainly a Paleozoic-early Tertiary sedimentary succession (principally shelf carbonates) with Neogene metamorphic core complexes at higher elevations (Hodges et al., 1996). The glacier snout has retreated about 1 km from its terminal moraine at the floor of the main Marsyandi valley, a distance that is about half as far as the distance that the nearby, and significantly larger Gangapurna Glacier has retreated since 1957 (Hagen, 1969). Milarepa's Glacier is bounded by two large lateral moraines (Figs. 1b and 3), which separate the valley sidewalls from the glacier surface (Fig. 4). Morphologically, the moraines are well developed and due to their sharp crests and relatively un-dissected sides, appear to be neo-glacial. Extensive and systematic observations of the ice in crevasses below the bergschrund and at the terminus, shows little to no debris entrainment within the glacier (Fig. 5), although the presence of the bergschrund and the processes of debris contribution to the glacier suggests that some debris must be entrained and is emergent due to ablation as well as the glacial flow paths (e.g. Small, 1987a; Anderson, 2000). As a first-order approximation, we assume that all supraglacial debris originates from the headwall (Figs. 1b and 2) rather than being eroded from the base of the glacier and that relatively little debris is entrained in the ice (e.g. Potter et al., 1998). While the

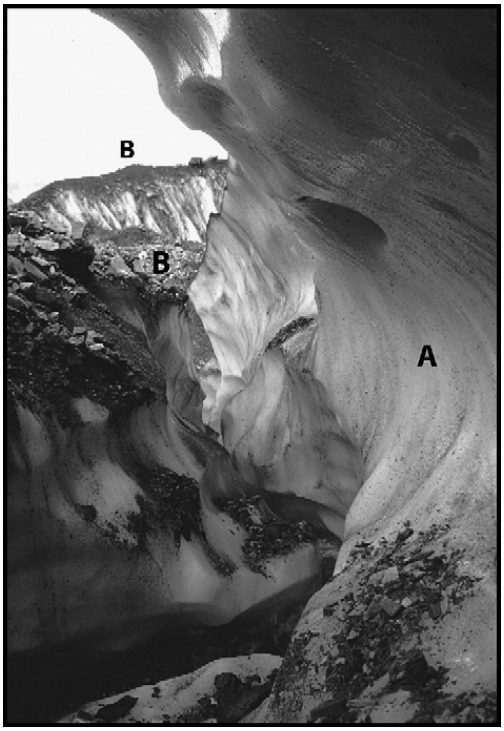

Fig. 5. Photograph within a crevasse draining into a moulin on the surface of the glacier roughly 1 km downslope of the bergschrund separating the glacier from the headwall. Note clean glacier ice (A) and thin layer of supraglacial debris (B) mantling the surface of the glacier.

glacier as retreated significantly such that it is now inset into its lateral moraines, the sharp moraine crests and minimal talus piles at base of the moraines suggests that the moraines are a relatively small source of supraglacial debris.

3.2. Supraglacial debris and headwall retreat

We measured downslope movement of the glacier surface using five stable locations (large, well entrenched boulders) at different locations on the glacier surface. These points were re-occupied with a Trimble differential GPS RTK Total Station® 4700 every 3–5 days until the satellite signal was stable enough to insure sub-centimeter-scale accuracy at each point. Using the GPS Total Station, we determined the horizontal and vertical position of each point over time relative to a fixed base station that was left in place for the duration of the field season (about 3 months). We used these measurements to calculate slope-parallel movement rates (distance traveled downslope divided by time between measurement) of the glacier surface, which correspond to the downslope transport rate of the supraglacial material debris.

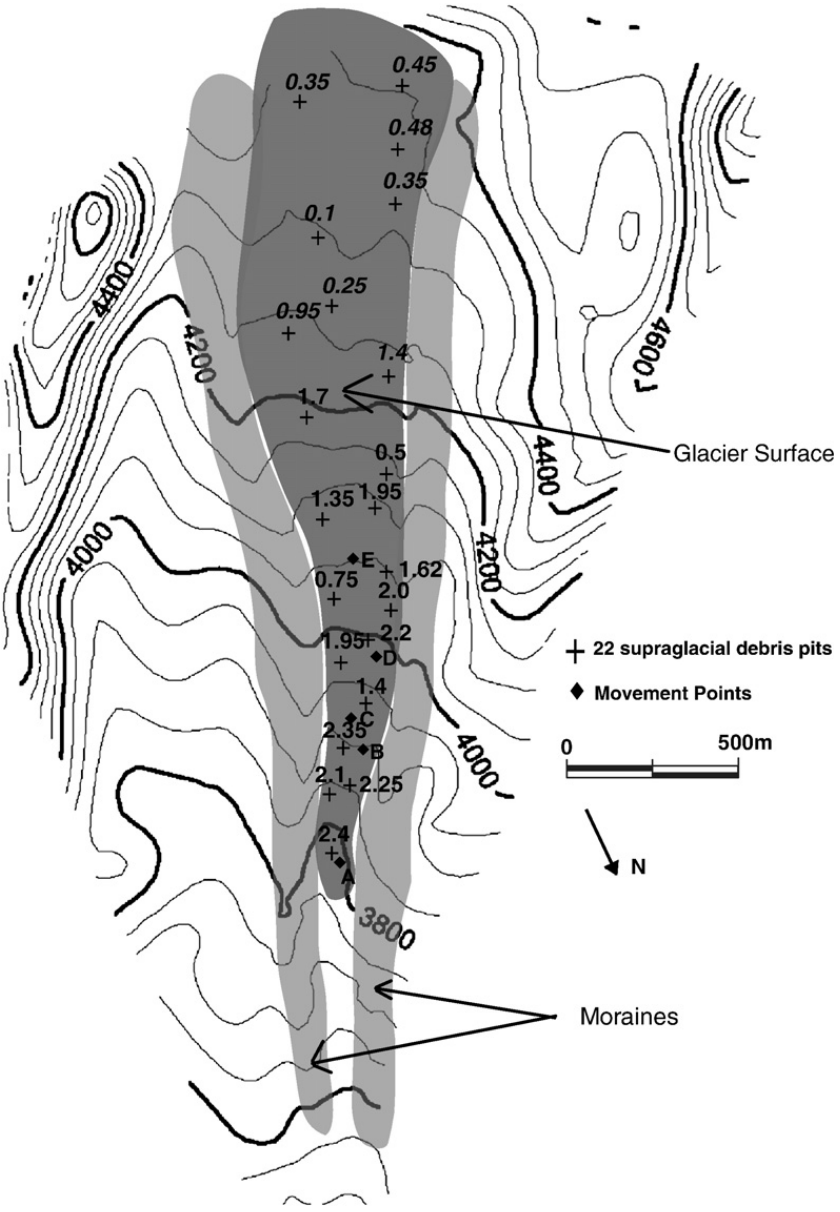

Fig. 6. Topographic map of study area created from field surveying using a Trimble GPS RTK Total Station® 4700 showing locations of supraglacial debris depth measurements (black crosses) with debris depths (m) labeled above or to the right of symbols. Stable points used to measure glacial movement are shown by the filled black diamonds and the letter labeling them corresponds to letters in Table 1. Headwall topography and the upper accumulation area are omitted for clarity. Elevations noted in m asl for the dark contour lines at 200 m intervals.

We measured supraglacial debris depths by digging pits with a shovel and pick-axe across the surface of the glacier (Fig. 6). Using the pits, we measured the vertical depth of debris cover with a tape measure. We estimated the porosity within the debris mantle to be about 10% across all our pits, reflecting the mixed fine and coarse sizes in the debris cover. We also surveyed the surface of the glacier and the surrounding catchment topography over the course of the summer (June–August) field season using differential GPS (Figs. 2 and 6). While our measured depths spanned the entire length of the ablation zone of the glacier, we used only local debris depths for each of the surveyed base stations to determine the local sediment transport flux. Debris cover across this region was relatively consistent such that our depth measurements from pits were applicable across local widths of the glacier surface. The measured surface velocity of the ice multiplied by the cross sectional area of the debris cover (average local debris depth times the width of the debris cover at each velocity measurement point) enabled a yearly volumetric flux of supraglacial debris. We determined a headwall retreat rate by dividing this volumetric flux by the contributing surface area of the headwall and correcting for inflation (i.e. change in bulk density between bedrock and sediment mantle). We note again that this calculation leads to a surface-perpendicular erosion rate rather than a vertical lowering rate (the common way to report erosion rates) or a horizontal retreat rate (the common way to report headwall retreat rates). We therefore convert the surface-perpendicular erosion rates to both horizontal and vertical rates using the average gradient of the contributing area (Nepal, 2001).

3.3. Cosmogenic nuclides

We used a hammer and chisel to sample the top 1 to 3 cm of the sample sites where we could find sufficient quartz for cosmogenic nuclide analyses on the ridge crests and at sidewall rock outcrops. We also collected surface samples (1 to 3 cm) from large boulders on the lateral moraine crests by the same method. Aggregate samples were also collected from the moraine crests and supraglacial debris to provide an average exposure age in locations where there were no suitable boulders for dating. Similarly, we also collected samples of large boulders and aggregates of cobbles from the surface of the glacier. Sample sizes ranged from 1 kg, for samples with relatively high quartz content, to 2 kg for samples with less quartz to ensure at least 150 g of separated and purified quartz, the target mineral for in situ cosmogenic nuclide studies. The latitude, longitude, elevation, aspect and shielding were recorded for each of the samples (Dunai, 2000; Gosse and Phillips, 2001) using the differential GPS that we used for our topographic surveys. We calculated a site specific nuclide production rates using a base production rate for ^{10}Be of 5.1 ± 0.3 atoms/g/yr calculated for sea level at 60° N (Stone, 2000). Samples were assumed to be too young (moraine crests samples, supraglacial debris samples) or eroding too fast (bedrock samples) for measurements of ^{26}Al to yield meaningful information on the exposure history of the samples using the ratio of ^{26}Al to ^{10}Be as described in Nishiizumi et al. (1991).

Where possible, we collected samples from near horizontal positions to maximize the exposure of the surface to the cosmic ray flux. Nishiizumi et al. (1989) discuss the implications of sampling inclined surfaces and production rates were corrected for the effects of dipping surfaces as well as for topographic shielding after Stone (2000) and Dunai (2000). The potential effects of snow cover were calculated based upon snow data for weather stations at similar elevations on the north slope of the Annapurna Range (Putkonen, personal communication) and found to be negligible. We attempted carefully to collect samples from locations that had not obviously failed recently by blockfall as the nuclide concentrations would not reflect a steady-state erosional process.

4. Results and discussion

4.1. Headwall retreat rate

The twenty-two pits dug across the surface of the glacier (Fig. 6) show debris cover depths ranging from 0.1 m to 2.4 m, yielding an average supraglacial debris depth of 1.3 m for the glacier surface away from any sediment input from the moraines. We observe an increase in debris depth down-glacier with locally thin and thick regions of cover, which we interpret to reflect the significant narrowing of the constraining valley formed by the lateral moraines, rather than the addition of significant englacial debris in the ablation area. The upper, gentler portion of the glacier has significantly thinner debris cover with an average depth of 0.7 m while the lower, steeper portion of the glacier has an average debris depth of 1.8 m. Surface movement rates for all six re-occupied sites averaged to 0.047 ± 0.006 m/day, with little variation between sites (Table 1). Average daily movement rates ranged from 0.045 m/day at site E to 0.050 m/day for sites B and D. Individual measurements of movement rates varied from 0.031 m/day to 0.058 m/day

Table 1
Supraglacial debris transport

Site A downslope			Site B downslope			Site C downslope		
#days [a]	Movement (m) [b]	Rate (m/day) [c]	#days	Movement (m) [b]	Rate (m/day)	#days	Movement (m) [b]	Rate (m/day)
5	0.276	0.055	5	0.266	0.053	5	0.247	0.049
4	0.214	0.054	4	0.226	0.057	4	0.208	0.052
4	0.159	0.040	4	0.167	0.042	4	0.124	0.031
3	0.156	0.052	3	0.122	0.041	3	0.144	0.048
6	0.272	0.045	6	0.346	0.058	6	0.317	0.053
16	0.75	0.047	16	0.794	0.050	16	0.736	0.046
	Average	0.049		Average	0.050		Average	0.047
Width (m)	100		Width (m)	148		Width (m)	185	
Depth (m)	2.4		Depth (m)	2.4		Depth (m)	1.8	

Site D downslope			Site E downslope				
#days	Movement (m) [b]	Rate (m/day)	#days	Movement (m) [b]	Rate (m/day)	Site	Flux (m 3/yr)
4	0.172	0.043	4	0.189	0.047	A	4290
3	0.126	0.042	3	0.139	0.046	B	6350
6	0.312	0.052	6	0.257	0.043	C	5720
16	0.787	0.049	16	0.67	0.042	D	7624
	Average	0.047		Average	0.045	E	5110
Width(m)	222		Width (m)	259		Average	5820
Depth (m)	2.0		Depth (m)	1.2			

[a] # days refers to the time between re-occupation of movement points.
[b] Downslope movement is relative to a fixed base station and corrected for local slope.
[c] Glacial movement rates determined from repeated GPS surveying of stable locations across the glacier.

(Table 1). Velocity vectors for all survey sites are oriented in the same direction and show the glacier surface movement to be N 10°E (Fig. 6). While the internal agreement between each of these survey points is encouraging, there is likely to be considerable variation in downslope transport rates depending on season. We discuss the potential range of transport rates below by presenting an estimate of the long-term transport rate of supraglacial material.

Using the slope parallel local debris transport velocity measurements for each of the stable surveyed points (Table 1), with measured width and depth of the debris (Table 1, Fig. 6), we estimated the supraglacial debris flux for cross sections across the glacier at each of the velocity measurement sites. Assuming that the average velocity measured during the field season equals the average annual transport velocity, the local flux ranges from 4290±640 m^3/yr near the terminus to 7620±1140 m^3/yr about 100 m in elevation higher up the glacier. There is no systematic variation of flux with distance downslope, or width of the cross section, and if we assume roughly the same velocity for the debris transport for the upper portions of the glacier we find similar variations of flux (i.e. from 3810 to 6350 m^3/yr for cross sections with widths and depths of 0.4 m and 560 m, and 1 m and 370 m, respectively. We therefore use the average transport flux of 5820±1990 m^3/yr from all five of the velocity measurement sites to estimate the erosion rate of the headwall. This flux was corrected for the change in bulk density between the bedrock source area of the headwall and the supraglacial debris mantle using an estimated sediment to rock ratio of 0.8.

Dividing the average transport flux 5820±1990 m^3/yr by the contributing surface area of the main headwall bowl, 4.5 km^2, yields a surface-perpendicular erosion rate of 1.3±0.5 mm/yr. If we include the side slopes, with a additional contributing surface area of 2.6 km^2, that might be supplying debris to the surface of the glacier, the inferred surface-perpendicular erosion rate drops to 0.82±0.3 mm/yr. Based on our observations of minimal debris contributions from the side slopes, we use the contributing area of the main bowl for the best estimate of a maximum headwall retreat rate. This estimated rate is likely to be an upper bound on the long-term average rate as our field season was during the summer when glacial movement due to sliding and deformation is likely to be the highest. Without detailed measurements throughout the year on Milarepa's glacier, we cannot be certain of a long-term average rate of downslope transport, but we estimate a range of potential velocities below, based on our cosmogenic nuclide exposure ages of supraglacial debris and note

that temporal variations in glacier motion can be quite significant.

The average gradient across the main headwall area that is contributing sediment to Milarepa's glacier is 1.24. Using this gradient with the maximum slope-perpendicular erosion rate of 1.3±0.5 mm/yr yields a vertical lowering rate of 0.42±0.16 mm/yr, and a horizontal retreat rate of 1.2±0.5 mm/yr.

The headwall retreat rates inferred here are within the range of about 0.1 to 1.0 mm/yr reported elsewhere for periglacial environments (French, 1996), and are well within the range reported for areas dominated by active rock glaciers (e.g. Gray, 1970; Barsch, 1977a; Buchenauer, 1990). It is, however, the first such rate determined for the Nepal Himalaya. Studies in periglacial environments are often limited to seasonal observations of rockfall on snow (e.g. Matsuoka and Sakai, 1999) and may not be representative of average rockfall activity on a multi year timescale. Our method integrates over hundred-year to millennial timescales and therefore incorporates higher magnitude, lower frequency events triggered by earthquakes, or years with intense precipitation that may have triggered increased rockfall activity (e.g. Matsuoka, 1990). We do not, however, assume this rate to be representative of a retreat rate applicable over the last several thousand years, nor is it thought to be representative of retreat rates for potential future climates. Instead, it is a first-order estimate based on assumptions reasonable for the field conditions that we observed and is likely to be constrained further through continued investigation. We discuss below how our short-term measurements of supraglacial sediment transport rates may overestimate of the down-glacier debris flux rates.

An additional source of uncertainty in estimating headwall retreat rates from the flux of supraglacial debris is the additional debris transported englacially (e.g. Benn and Evans, 1998). We attempted to use ground penetrating radar to estimate ice thickness and englacial debris concentrations (e.g. Gades et al., 2000), but were unsuccessful in obtaining meaningful results. Our field observations suggested minimal englacial transport, which is the assumption we used. If we use a conservative estimate of englacial debris concentration of 10% by volume (e.g. Hunter et al., 1996) and a rough estimate of ice cross-sectional area at measurement site C (Table 1) of 3700 m^2 (185 m wide by 20 m deep, on average), then we would estimate a englacial sediment transport flux comparable to the supraglacial flux. This additional sediment transport flux would be halved if we estimated the average

Table 2
^{10}Be exposure ages

Sample ID[4]	Sample	Elevation (m)	^{10}Be (atoms/g)	Error[1]	Production rate[2] (atoms/g–yr)	Exposure age (yr)	±yr
NP 222	*E moraine crest*	4000	4.348E+04	6.51E+03	55.21	788	127
NP 223	E moraine crest	3813	2.306E+04	3.62E+03	50.11	460	77
NP 233	E moraine crest	4275	1.509E+04	3.38E+03	63.4	238	55
NP 234	E moraine crest	4216	2.483E+04	1.99E+03	63.4	392	40
NP 235	E moraine crest	4157	7.401E+03	6.47E+02	59.79	124	13
NP 212	W moraine crest	3844	2.646E+04	1.62E+03	50.93	520	44
NP 213	W moraine crest	3797	7.042E+03	1.78E+03	49.69	142	37
NP 214	W moraine crest	3669	1.981E+04	1.40E+03	46.43	427	39
NP 215	Glacier surface	4288	1.527E+04	2.25E+03	63.81	239	38
NP 216	*Glacier surface*	4288	5.716E+04	*9.00E+03*	*63.81*	*896*	*151*
NP 217	Glacier surface	4217	1.798E+04	4.37E+03	61.61	292	73
NP 218	Glacier surface	4062	1.995E+04	2.17E+03	56.99	350	43
NP 220	*Glacier surface*	3921	4.308E+04	*4.09E+03*	*53.01*	*813*	*91*
NP 221	Glacier surface	3862	1.440E+04	9.96E+02	51.41	280	25
NP 225	Glacier surface	3800	2.205E+04	1.89E+03	48.14	458	46
NP 226	Glacier surface	3862	1.814E+04	1.20E+03	51.41	353	31
NP 227	Glacier surface	4000	2.185E+04	1.96E+03	51.41	425	42
NP 228	*Glacier surface*	4000	2.405E+03	*1.50E+03*	*51.41*	*47*	*27*
NP 229	Glacier surface	4000	7.467E+03	1.45E+03	51.41	145	135
NP 230	*Glacier surface*	4306	5.396E+04	*3.10E+03*	*64.38*	*838*	*69*
NP 231	Glacier surface	4306	1.193E+04	8.48E+02	64.38	185	17
NP 232	Glacier surface	4306	7.422E+03	7.51E+02	64.38	115	13

[1]Errors represent 1σ analytical uncertainties.
[2]Production rates scaled by base production rate of 5.1±0.3 atoms/g/yr for sea level at 60°N (Stone, 2000).
[3]Samples in italics are not used in calculations of moraine age or long-term supraglacial.
[4]Latitude, longitude, elevation, aspect and shielding recorded for all samples (Dunai, 2000; Gosse and Phillips, 2001).

Table 3
Inferred ^{10}Be erosion rates

Sample ID[4]	Sample description	Elevation (m)	^{10}Be (atoms/g)	Error[1]	Production Rate[2] (atoms/g–yr)	Erosion rate (mm/yr)	± (mm/yr)
NP 236	Ridge crest	4069	3.36E+05	1.88E+04	57.19	0.101	0.018
NP 239	Ridge crest	4723	2.33E+05	1.36E+04	78.60	0.200	0.037
NP 240	*Ridge crest*	4897	2.16E+04	*1.47E+03*	*78.42*	*2.150*	*0.410*
NP 241	Ridge crest	4718	1.51E+06	8.88E+04	17.07	0.006	0.003
NP 242	Ridge crest	4858	4.35E+05	2.42E+04	17.07	0.023	0.011
NP 203	Valley sidewall	4288	1.42E+05	7.90E+03	61.95	0.259	0.047
NP 205	Valley sidewall	4302	1.80E+05	1.00E+04	64.25	0.211	0.038
NP 206	Valley sidewall	4540	2.96E+05	1.72E+04	72.11	0.144	0.026
NP 211	*Valley sidewall*	4610	3.36E+04	*2.16E+03*	*74.54*	*1.310*	*0.250*

[1]Errors represent 1σ analytical uncertainties.
[2]Production rates scaled by base production rate of 5.1±0.3 atoms/g/yr for sea level at 60° N (Stone, 2000).
[3]Samples in italics interpreted as recent blockfall failure.
[4]Latitude, longitude, elevation, aspect and shielding recorded for all samples (Dunai, 2000; Gosse and Phillips, 2001).

ice depth to be 10 m, or the englacial debris concentration to be 5%. The resulting headwall retreat rate estimate would be increased by a factor of 1.5 to 2 based on such accounting for englacial debris transport. Without the detailed measurements of englacial debris concentrations used in very few studies (e.g. Hunter et al., 1996) we cannot be certain about how much sediment is being transport within the glacier, but we do know that our estimate of headwall retreat using supraglacial transport alone is likely to be an underestimate.

4.2. Cosmogenic nuclide determined exposure ages

We analyzed a total of thirty-one samples for ^{10}Be concentrations (sample locations shown in Fig. 2, inset): eight samples from moraine crests (east and west) for exposure age dating; fourteen from the debris on the surface of the glacier for exposure age dating; five samples from exposed bedrock on ridge crests for determining erosion rates; and, four bedrock samples from the valley sidewalls, also for determining erosion rates (Tables 2 and 3).

Measurements of ^{10}Be concentrations from the moraine crest samples led to us to infer minimum exposure ages ranging from 124±13 to 788±127 yr (Fig. 7, Table 2). West moraine crest samples led to an average minimum exposure age of 363±40 yr, while east moraine crest samples yielded an average minimum exposure age of 400±62 yr. The three aggregate samples, with minimum exposure ages ranging from 392±40 to 520±42 yr, yielded an average of 446±41 yr. The samples collected from individual boulders show greater scatter, ranging from 124±13 yr to 788±127 yr with an average minimum exposure age of 350±62 yr.

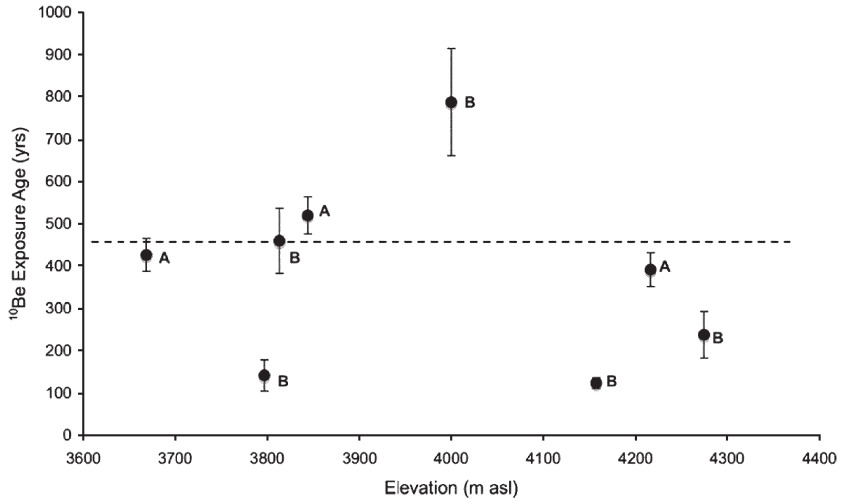

Fig. 7. Exposure ages inferred from measured ^{10}Be concentrations from samples on the east and west lateral moraine crests as a function of elevation. Age spread is similar for both moraines and so the symbols are not differentiated. The letters beside the symbols designate whether the sample was an aggregate (A) or boulder (B). Dashed line represents moraine age of 468 yr based upon method of Putkonen and Swanson (2003).

There is a relatively high degree of scatter in the inferred moraine crest exposure ages (Fig. 7). Putkonen and Swanson (2003) suggest that cosmogenic dating of moraines is complicated by erosion of the moraine and subsequent exposure of boulders, yielding ages generally younger than the moraine itself. They also suggest that to get an accurate age for moraines with initial heights of 30 m and ages younger than 20 kyr, at least five samples should be analyzed. Based upon the intact morphology of the moraines we suggest that the moraines are younger than the inferred exposure age of a large boulder sample, NP222, and that its relatively old exposure age (788±127 yr), determined by relatively high nuclide concentrations, may be the result of pre-deposition exposure (Fig. 7). We therefore do not include this sample in our interpretation of the moraine samples. The remaining seven samples show a large range in exposure ages consistent with the findings of Putkonen and Swanson (2003), who show an on-site average age range of 38% for all published cosmogenic exposure ages for moraines, suggesting that age of the oldest boulder on the moraine will be ≥90% of the moraine age. Using their method yields a minimum moraine age of 468 yr, which is consistent with the 480±80 year time of a glacial advance for the Imja Khola Basin, Khumbu Himalaya, Nepal, roughly 200 km east of our field area, but with a similar climatic setting, as determined by radiocarbon dating (Fushimi, 1978). This close agreement between different field sites in the Greater Himalaya of Nepal suggests that there may have been a significant regional period of glacial expansion for the Himalayas around 460–480 yr, about the time of the Little Ice Age (roughly 450–300 yr ago).

We observed a similar range of exposure ages using ^{10}Be concentrations inferred from samples from the surface of the glacier (Fig. 8). Aggregate sample concentrations lead to an inference of minimum exposure ages ranging from 115±13 to 896±151 yr with an average minimum exposure age of 460±50 yr. Concentrations from individual boulder samples lead to minimum exposure ages that range from 145±135 to 810±90 yr with an average age of 330±70 yr.

We estimate the residence time of the supraglacial debris in the glacial system by dividing the slope length of the glacier (4400 m) by the short-term surface movement rate determined above (17 m/yr), assuming that this short-term rate is constant. This first-order estimate yields a residence time for sediment of about 260 yr as it travels from headwall to terminus, suggesting that, if this short-term rate were applicable over longer time scales, exposure ages should range from zero near the headwall to 260 yr at the terminus. We plot nuclide-inferred exposure ages against slope distance, where our lowest sample is about 200 m upslope of the terminus and our highest sample is at 4300 m, on the broad, low-gradient area prior to the break in slope between accumulation and ablation areas and about 1500 m downslope from the bergschrund (Fig. 8). If sediments were indeed being transported at 17 m/yr, the highest elevation samples would yield exposure ages of about 90 yr, while the lowest elevation sample would yield an exposure age of about 260 yr.

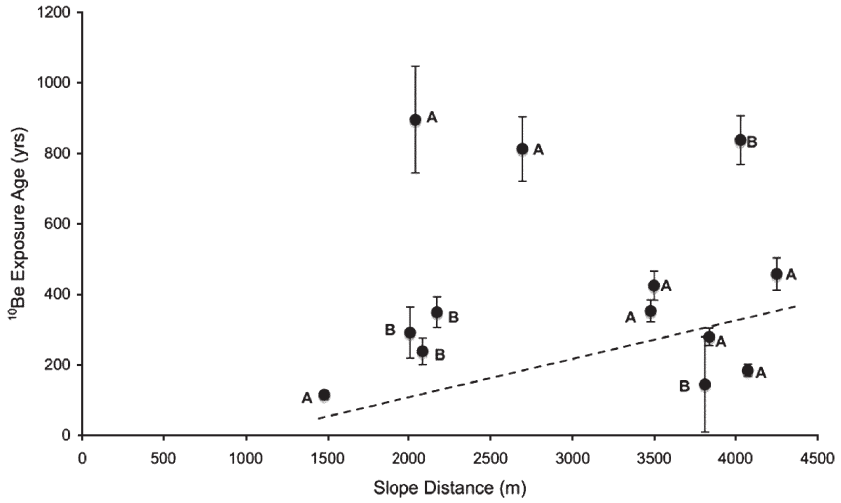

Fig. 8. Exposure ages inferred from measured ^{10}Be concentrations from boulders and aggregate samples from the supraglacial surface of the glacier as a function of slope distance from the uppermost extent of the glacier. Samples are noted by letter to differentiate aggregate (A) samples of small cobbles and tops of boulders, from boulder (B) samples of only boulder tops. Trend line shows a rough fit to the average long-term rate of downslope movement of 10 m/yr. Excluding the three oldest samples (>800 yr exposure ages) that are likely to have some inheritance from prior exposure increases this inferred long-term rate to 12 m/yr.

Instead, we infer exposure ages for the highest samples that range from 115 to over 800 yr, and infer an exposure age of 460 yr for the lowest elevation sample.

This scatter in ^{10}Be exposure ages for the supraglacial debris can be explained by the potentially different and complicated exposure histories of these samples. Supraglacial debris surfaces are unstable and therefore samples may be buried or shielded periodically by other debris as they are transported. This process would result in the inference of younger exposure ages than their actual exposure history by shielding the boulders from incoming cosmic ray flux. Additionally, samples may have had different exposure histories prior to reaching the surface of the glacier and the significantly higher nuclide production rate on rock sourced from the contributing area cliff faces will also change the inferred ages measured if there is any inherited nuclide concentration. Finally, during down-glacier transport, boulders and other supraglacial debris may be eroded such that any accumulated nuclide concentrations may include an erosional history. For the most part, these factors would lead to exposure ages younger than the age inferred from nuclide concentrations accumulated during transit upon the glacier's surface.

The data plotted on Fig. 8 show the reality of sampling on such a complicated surface, even when we used aggregate samples to help minimize such differences in exposure history. One end-member interpretation of these data would be to suggest that there was some catastrophic failure of the headwall, perhaps roughly coincident with the age of the moraines, which deposited most of the supraglacial debris. The debris has been smoothing itself down-glacier and exposure ages reflect the wide range of scatter around some input age, perhaps about 450 yr ago. Another way to interpret these data is to exclude anomalously old samples (>800 yr) that were likely to have had some inheritance prior to deposition (Fig. 8). The remaining age vs. slope distance data reveal a rough increase in age with distance down glacier. Using these data with the downslope transport distance of the samples yields an estimated long-term transport rate of about 10 m/yr. Using the older samples, near the terminus of the glacier, leads to a calculated residence time of about 440 yr for the length of the glacier. While this is a rough estimate based on these exposure ages, it is encouraging that it is not only reasonably slower than the short-term rate, but also of the same magnitude (e.g. Benn and Evans, 1998). If this long-term rate is correct, then the slower transport rate would result in a reduced supraglacial sediment flux of 3800 m^3/yr, which would lead to an inference of a slope-perpendicular erosion rate of the headwall of 0.82±0.31 mm/yr for the same contributing area. This would lead to a vertical lowering rate of 0.25±0.10 mm/yr, which is remarkably similar to the cosmogenic nuclide determined erosion rates for the bedrock sidewalls, discussed below.

4.3. Cosmogenic nuclide determined and erosion rates

Measured concentrations of ^{10}Be from the five ridge crest bedrock samples led us to infer erosion rates ranging from 0.006±0.003 mm/yr to 2.15±0.41 mm/yr using Equation 6, while ^{10}Be concentrations from the four sidewall bedrock samples yielded erosion rates ranging from 0.14±0.03 to 1.31±0.25 mm/yr (Fig. 9, Table 3). These rates are equivalent to vertical lowering rates. Samples NP211 (from the valley sidewall) and

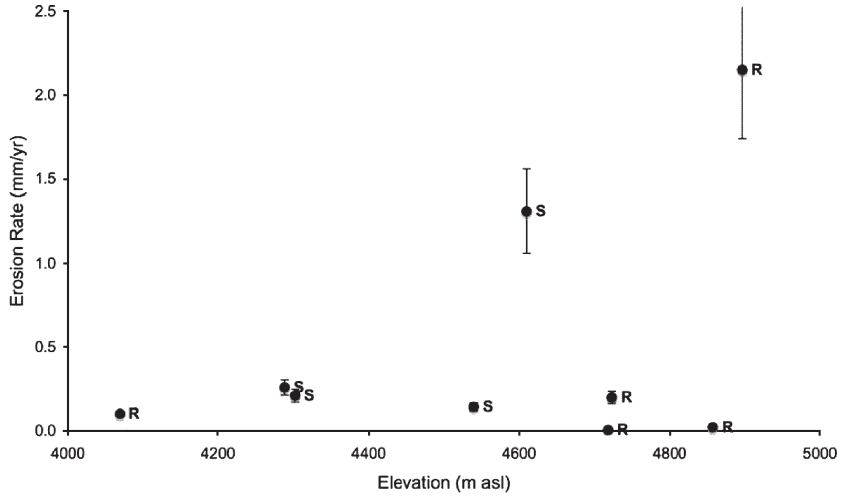

Fig. 9. Inferred erosion rates (mm/yr) from ^{10}Be concentrations for ridge crest (R) and valley sidewall (S) bedrock samples plotted against elevation (m asl). Note that the two highest erosion rates are determined from samples thought to have experienced recent blockfall failure.

NP240 (from the eastern ridge crest, approximate location shown on Fig. 1b), with erosion rates of 1.31±0.25 mm/yr and 2.15±0.41 mm/yr respectively, are from narrow, highly exposed bedrock surfaces. NP240 is from between two bedrock exposures on a narrow ridge and was the only quartz-bearing rock available on the high ridge. NP211 is from the exposed bedrock above the head of the glacier. Both samples are likely to reflect non-steady-state erosional histories and were noted as potential outliers in our sample notes. Excluding these two samples, which were very likely to have experienced recent block erosion, there is remarkable agreement between samples across the study area. The average erosion rate is 0.08±0.03 mm/yr for the bedrock ridges, and is 0.20±0.05 mm/yr for the valley sidewalls. Sample NP 236 with an erosion rate of 0.10±0.02 mm/yr is the lowest elevation ridge crest sample collected and is from a horizontal surface on the western ridge (Fig. 1b). Samples NP239, NP241, and NP242, are from narrower ridge crests at higher elevations. The two samples (NP241 and NP242) from the highest elevations show the lowest erosion rates (0.006±0.003 and 0.023±0.011 mm/yr respectively).

Despite the rough agreement, our results show a large range of erosion rates for different parts of the landscape from 0.006±0.003 mm/yr to 2.15±0.41 mm/yr (Fig. 9). The high inferred erosion rates for samples NP211 and NP240 (1.31±0.25 mm/yr and 2.15±0.41 mm/yr respectively), as well as sample morphology and location, suggest that these samples may be from locations eroding through blockfall that were recently exposed (T_{eff} for NP211 and NP240 is 451±39 yr and 275±25 yr, respectively). Nuclide concentrations from these samples may not represent steady-state erosional histories and were therefore sampled inappropriately despite our best attempts to constrain our samples in the field. Conversely, sample NP236, taken at the lowest elevation, with an erosion rate of 0.10±0.02 mm/yr, is from a broad, flat, grass covered, convex ridge that is unlikely to experience any blockfall or landslide. The results for bedrock ridge crest erosion rates reported here are significantly faster than erosion rates reported for alpine environments in other mountain ranges (e.g. Small et al., 1997; Summerfield et al., 1999). While it may be tempting to link the high uplift rates of the Himalaya to these rates, the ridge crest morphology and erosional processes are not significantly different at our field site than at other alpine sites, which raises an interesting paradox.

We suggest that our site may be subjected to more extreme climate variations due to the high elevation and the role of the monsoon, but the direct connections between climate and erosional processes and rates have yet to be realized (e.g. Burbank et al., 2003; Hodges et al., 2004; Wobus et al., 2005). Nishiizumi et al. (1993) report bedrock ridge crest erosion rates based on two measurements from the Tibetan Plateau, north of our study area and in a very different climatic setting, of 0.014 mm/yr and 0.056 mm/yr. These rates are on average much lower than those reported here, but sample details are lacking from their study except that they were well into the rain shadow of the Himalaya. Our two ridge crest with the lowest rates (0.006±0.003 and 0.023±0.011 mm/yr) fall below and within the rates reported by Nishiizumi et al. (1993). Despite the range of rates inferred by our samples, we suggest that ridge crests are lowering at an average of 0.08±0.03 mm/yr, while the sidewalls are eroding more rapidly, at an average of 0.20±0.05 mm/yr.

If we use our long-term estimate of down-glacier sediment transport rates determined from exposure age dating of the supraglacial debris, then the vertical lowering rate due to headwall retreat approaches the average sidewall erosion rate. If this is indeed the case, then it is likely that the bedrock erosion rates across the up-glacier slopes of our field site are roughly similar and that processes of catastrophic blockfall are ultimately setting the lowering rate of the ridge crests. While the processes eroding the exposed bedrock walls of the study area are periglacial (e.g. frost cracking, ice wedging), the resulting blockfall erosion contributing sediment to the glacier surface is being driven by the incision of the glacier on the valley floor. It is unlikely that this valley has been free from glacial cover during its evolution and the absence of an overdeepened gorge suggests that the glacier is not eroding significantly faster than the surrounding valley walls (Fig. 1b). If this is indeed the case, then our quantification of periglacial erosion rates offer some constraint on glacial erosion rates for small alpine glaciers in the Nepal Himalaya. If so, then both periglacial rates and the inferred glacial rates quantified here are significantly lower than the few fluvial incision rates that have been estimated for trans-Himalayan rivers.

Fluvial incision rates determined for the Himalaya range from 1–12 mm/yr (Leland et al., 1998; Pratt et al., 2002; Pratt-Sitaula et al., 2004) and depend on tectonic setting. Using the maximum rate of 8.5 mm/yr estimated for the region (Pratt-Sitaula et al., 2004) suggests that erosion of the ridge crests, valley sidewalls, and the main headwall of Milarepa's Glacier is unable to keep pace with fluvial incision downstream in the Marsyandi River, and that relief must be increasing with time. If such high incision rates continue over time, propagating up the Marsyandi drainage, they would lead to long,

over-steepened hillslopes that are less stable and subject to increased denudation by bedrock landsliding (e.g. Schmidt and Montgomery, 1995). Whipple et al. (1999) suggest, however, that an increase in fluvial erosion does not necessarily lead to an increase in relief due to the supposed onset of catastrophic failure collapsing the over-steepened slopes. Because ridge crest lowering is unable to match fluvial incision rates the resulting over-steepened slopes are likely to be subject to large-scale collapse such as the valley filling events suggested by Pratt et al. (2002). At this point we are unable to distinguish between the roles of fluvial and glacial erosion in setting the base level for the surrounding landscape, but given the results reported here and forthcoming glacial chronologies (Pratt-Sitaula et al., 2003), we suggest a full-scale morphologic analysis for the region, similar to Brocklehurst and Whipple (2002), will help resolve this fundamental question.

5. Conclusions

We present a method for determining headwall retreat rates based upon measuring the flux of supraglacial debris eroded from a bedrock-dominated headwall. We applied our method to a small debris covered glacier in the central Nepal Himalaya, calculating a sediment flux of 5820±1990 m^3/yr, which led to determining a slope-perpendicular headwall retreat rate of 1.3±0.5 mm/yr, well within rates reported using other methods in a variety of settings. This slope-perpendicular rate corresponds to a vertical lowering rate of 0.42±0.16 mm/yr and a horizontal retreat rate of 1.2±0.5 mm/yr. Cosmogenic nuclide concentrations (^{10}Be) from bedrock ridge crest and valley sidewalls inferred average point specific erosion rates of 0.08±0.03 mm/yr and 0.20±0.05 mm/yr, respectively, which are equivalent to vertical lowering rates. Differences between these nuclide-derived rates and the flux-derived rate is likely due to uncertainties in both the headwall contributing area, as well as the downslope transport flux of the supraglacial debris. We estimate a long-term transport sediment transport rate by the glacier by dating supraglacial debris with ^{10}Be measurements, which reduces the slope-perpendicular erosion rate of the headwall to 0.82±0.31 mm/yr for the same contributing area. This would lead to a vertical lowering rate of 0.25±0.10 mm/yr, comparable to the erosion rates for the valley sidewalls determined using cosmogenic nuclide analyses. If this were the case, then the headwall and sidewalls would be eroding at roughly similar rates. We also use cosmogenic nuclide concentrations from moraine crest samples to determine that a significant glacial advance in the region occurred about 470 yr ago and therefore corresponds to the onset of the Little Ice Age in Europe. Finally, we compare our point-specific erosion rates to fluvial incision rates for the Marsyandi River draining the study area and a similarly steep region with active fluvial incision into bedrock gorges in the northwestern Himalaya and find a large discrepancy between fluvial incision and ridge crest and sidewall erosion rates. This comparison quantifies the morphologic suggestion that even over-steepened vertical rock faces responding to glacial incision are unable to match the rapid down-cutting rates of the major rivers draining the Nepal Himalaya.

Acknowledgements

We thank Ajay Sitaula and his team in Nepal for excellent logistical support during the 3 months spent in the field. N. Humphrey, D. Lawson, and D. Burbank helped in the development of the conceptual framework and with the interpretation of our data. S. Prestrud Anderson and S. Brocklehurst greatly improved previous versions of the manuscript and L. Owen and an anonymous reviewer helped improve this version. Cosmogenic nuclide measurements and field support were funded by NSF Continental Dynamics Program grant EAR-9909335. Analyses were partially performed under the auspices of the U.S. Department of Energy by LLNL under contract W-7405-Eng-48.

References

Anderson, R.S., 2000. A model of ablation-dominated medial moraines and the generation of debris mantled glacier snouts. Journal of Glaciology 51, 459–469.

André, M.F., 1997. Holocene rockwall retreat in Svalbard: a triple-rate evolution. Earth Surface Processes and Landforms 22, 423–440.

Barsch, D., 1977a. Ein permafrost profile aus graubunden, Schweizen Alpen. Zeitschrift für Geomorphologie 21, 79–86.

Barsch, D., 1977b. Nature and importance of mass wasting by rock glaciers in alpine permafrost environments. Earth Surface Processes and Landforms 2, 231–245.

Barsch, D., Jakob, M., 1998. Mass transport by active rockglaciers in the Khumbu Himalaya. Geomorphology 26, 215–222.

Benn, D.I., Evans, D.J.A., 1998. Glaciers and Glaciation. Arnold, London. 734 pp.

Benn, D.I., Lehmkuhl, F., 2000. Mass balance and equilibrium line altitudes of glaciers in high mountain environments. Quaternary International 65-66, 14–29.

Benn, D.I., Owen, L.A., 2002. Himalayan glacial sedimentary environments: A framework for reconstructing and dating the former extent of glaciers in high mountains. Quaternary International 97-98, 3–25.

Bhutiyani, M.R., 2000. Sediment load characteristics of a proglacial stream of Siachen Glacier and the erosion rate in Nubra valley in the Karakoram Himalayas, India. Journal of Hydrology 227, 84–92.

Bierman, P.R., Marsella, K.A., Patterson, C., Davis, P.T., Caffee, M., 1999. Mid-Pleistocene cosmogenic minimum-age limits for pre-Wisconsinan glacial surfaces in southwestern Minnesota and southern Baffin Island: a multiple nuclide approach. Geomorphology 27, 25–39.

Brewer, I.D., Burbank, D.W., Hodges, K.V., 2003. Modeling detrital cooling-age populations: insights from two Himalayan catchments. Basin Research 15, 305–320.

Brocklehurst, S.H., Whipple, K.X., 2002. Glacial erosion and relief production in the Eastern Sierra Nevada, California. Geomorphology 42, 1–24.

Brozovic, N., Burbank, D.W., Meigs, A., 1997. Climatic limits on landscape development in the northwestern Himalaya. Science 276, 571–574.

Buchenauer, H.W., 1990. Gletscher-und Blokgletschergeschichte der westlichen Schobergruppe (Osttirol). Marburger Geographischen Schriften 117 376 pp.

Burbank, D.W., Leland, D., Fielding, E., Anderson, R.S., Brozovic, N., Reid, M.R., Duncan, C., 1996. Bedrock incision, rock uplift and threshold hillslopes in the northwestern Himalayas. Nature 379, 505–510.

Burbank, D.W., Blythe, A.E., Putkonen, J., Pratt-Sitaula, B., Gabet, E., Oskin, M., Barros, A., Ojha, T.P., 2003. Decoupling of erosion and precipitation in the Himalayas. Nature 426, 652–655.

Caine, N., 1974. The geomorphic processes of alpine environments. In: Ives, J.D., Barry, R.G. (Eds.), Arctic and Alpine Environments. Methuen, London, pp. 721–748.

Church, M., Stock, R.F., Ryder, J.M., 1979. Contemporary sedimentary environments on Baffin Island, N.W.T Canada: debris slopes accumulations. Arctic and Alpine Research 11, 371–402.

Clark, D.H., Clark, M.M., Gillespie, A.R., 1994. Debris-covered glaciers in the Sierra Nevada, California, and their implications for snowline reconstructions. Quaternary Research 41, 139–153.

Collins, D.N., 1978. Quantitative determination of the subglacial hydrology of two alpine glaciers. Journal of Glaciology 23, 347–362.

Collins, D.N., 1998. Suspended sediment flux in meltwaters draining from Batura glacier as an indicator of the rate of glacial erosion in the Karakoram mountains. Journal of Quaternary Science 13, 1–10.

Douglas, G.R., 1980. Magnitude frequency study of rockfall in Co. Antrim, N. Ireland. Earth Surface Processes and Landforms 5, 123–129.

Dunai, T.J., 2000. Scaling factors for production of cosmogenic nuclides: a critical re-evaluation. Earth and Planetary Science Letters 176, 157–169.

French, H.M., 1996. The Periglacial Environment, 2nd edn. Longman, Essex. 341 pp.

Fujii, Y., Higuchi, K., 1977. Statistical analysis of the forms of the glaciers in the Khumbu Himal. Journal of Japanese Society of Snow and Ice (Seppyo) 39, 7–14.

Fushimi, H., 1978. Glaciations in the Khumbu Himal. Journal of Japanese Society of Snow and Ice (Seppyo) 40, 71–77.

Gabet, E.J., Burbank, D.W., Putkonen, J., Pratt-Sitaula, B.A., Ojha, T., 2004a. Rainfall thresholds for landsliding in the Himalayas of Nepal. Geomorphology 63, 131–143.

Gabet, E.J., Pratt-Sitaula, B.A., Burbank, D.W., 2004b. Climatic controls on hillslope angle and relief in the Himalayas. Geology 32, 629–632.

Gades, A., Conway, H., Nereson, N., Naito, N., Kadota, T., 2000. Radio echo-sounding through supraglacial debris on Lirung and Kuhmbu Glaciers, Nepal Himalayas. In: Nakawo, M., Raymond, C.F., Fountain, A. (Eds.), Debris-covered glaciers. Proceedings of a workshop held at Seattle, Washington, USA. IAHS Publ., vol. 264, pp. 13–22.

Galy, A., France-Lanord, C., 2001. Higher erosion rates in the Himalaya: geochemical constraints on riverine fluxes. Geology 29, 23–26.

Gosse, J.C., Phillips, F.M., 2001. Terrestrial in situ cosmogenic nuclides: theory and application. Quaternary Science Reviews 20, 1475–1560.

Gray, J.T., 1970. Mass wasting studies in the Ogilvie and Wernecke Mountains, Central Yukon Territory. Geological Survey Canada Papers 70-1, 192–195.

Hagen, T., 1969. Report on the Geological survey of Nepal. Denkschriften der Schweizerischen Naturforschenden Gesellschaft, vol. LXXXVI/I.

Hallet, B., Hunter, L., Bogen, J., 1996. Rates of erosion and sediment evacuation by glaciers: a review of field data and their implications. Global and Planetary Change 12, 213–235.

Harbor, J., Warburton, J., 1992. Glaciation and denudation rates. Nature 356, 751.

Harbor, J., Warburton, J., 1993. Relative rates of glacial and nonglacial erosion in alpine environments. Arctic and Alpine Research 25, 1–7.

Hodges, K.V., Parrish, R.R., Searle, M.P., 1996. Tectonic evolution of the central Annapurna Range, Nepalese Himalayas. Tectonics 15, 1264–1291.

Hodges, K.V., Wobus, C., Ruhl, K., Schildgen, T., Whipple, K., 2004. Quaternary deformation, river steepening, and heavy precipitation at the front of the Higher Himalayan ranges. Earth and Planetary Science Letters 220, 379–389.

Humlum, O., 2000. The geomorphic significance of rock glaciers: estimates of rock glacier debris volumes and headwall recession rates in West Greenland. Geomorphology 35, 41–67.

Hunter, L.E., Powell, R.D., Lawson, D.E., 1996. Flux of debris transported by ice at three Alaskan tidewater glaciers. Journal of Glaciology 42, 123–135.

Lal, D., 1988. In situ-produced cosmogenic isotopes in terrestrial rocks. Annual Review of Earth and Planetary Sciences 16, 355–388.

Lal, D., 1991. Cosmic ray labeling of erosion surfaces; in situ nuclide production rates and erosion models. Earth Planetary and Science Letters 104, 424–439.

Leland, J., Reid, M.R., Burbank, D.W., Finkel, R., Caffee, M., 1998. Incision and differential bedrock uplift along the Indus River near Nanga Parbat, Pakistan Himalaya, from ^{10}Be and ^{26}Al exposure age dating of bedrock straths. Earth and Planetary Science Letters 154, 93–107.

Matsuoka, N., 1990. The rate of bedrock weathering by frost action: field measurements and a predictive model. Earth Surface Processes and Landforms 15, 73–90.

Matsuoka, N., 1991. A model of the rate of frost shattering: application to field data from Japan, Svalbard and Antarctica. Permafrost Periglacial Processes 2, 271–281.

Matsuoka, N., Sakai, H., 1999. Rockfall activity from an alpine cliff during thawing periods. Geomorphology 28, 309–328.

Milliman, J.D., Syvitski, J.P.M., 1992. Geomorphic/tectonic control of sediment discharge to the ocean: the importance of small mountainous rivers. Journal of Geology 100, 525–544.

Molnar, P., England, P., 1990. Late Cenezoic uplift of mountain ranges and global climate change: chicken or egg? Nature 346, 29–34.

Montgomery, D.R., 2002. Valley formation by fluvial and glacial erosion. Geology 30, 1047–1050.

Moribayashi, S., 1974. On the characteristic of Nepal Himalayan Glaciers and their recent variation. Journal of Japanese Society of Snow and Ice (Seppyo) 36, 11–21.

Moribayashi, S., Higuchi, N., 1977. Characteristics of glaciers in the Khumbu region and their recent variations. Journal of Japanese Society of Snow and Ice (Seppyo) 39, 3–6.

Debris-covered glaciers. In: Nakawo, M., Raymond, C.F., Fountain, A. (Eds.), Proceedings of a workshop held at Seattle, Washington, USA. IAHS Publ., vol. 264. 288 pp.

Nepal, His Majesty's Government, 2001. 1: 50,000 scale map, Sheet No. 2884 05 (Chame), Survey Department, Kathmandu, Nepal.

Nishiizumi, K., Lal, D., Klein, J., Middleton, R., Arnold, J.R., 1986. Production of ^{10}Be and ^{26}Al by cosmic rays in terrestrial quartz in situ and implications for erosion rates. Nature 319, 134–136.

Nishiizumi, K., Winterer, E.L., Kohl, C.P., Klein, J., Middleton, R., Lal, D., Arnold, J.R., 1989. Cosmic ray production rates of ^{10}Be and ^{26}Al in quartz from glacially polished rocks. Journal of Geophysical Research 94 (B12), 17, 907–17, 915.

Nishiizumi, K., Kohl, C.P., Arnold, J.R., Klein, J., Fink, D., Middleton, R., 1991. Cosmic ray produced ^{10}Be and ^{26}Al in Antarctic rocks: exposure and erosion history. Earth and Planetary Science Letters 104, 440–454.

Nishiizumi, K., Kohl, C.P., Arnold, J.R., Dorn, R.I., Klein, J., Fink, D., Middleton, R., Lal, D., 1993. Role of in situ cosmogenic nuclides ^{10}Be and ^{26}Al in the study of diverse geomorphic processes. Earth Surface Processes and Landforms 18, 407–425.

Ono, Y., Watanabe, T., 1986. A protalus rampart related to alpine debris flows in the Kuranosuke Cirque, Northern Japanese Alps. Geografiska Annaler 68A, 213–223.

Owen, L.A., Finkel, R.C., Caffee, M.W., Gualtieri, L., 2002. Timing of multiple late Quaternary glaciations in the Hunza Valley, Karakoram Mountains, northern Pakistan: defined by cosmogenic radionuclide dating of moraines. Geological Society of America Bulletin 114, 593–604.

Owen, L.A., Derbyshire, E., Scott, C.H., 2003. Contemporary sediment production and transfer in high-altitude glaciers. Sedimentary Geology 155, 13–36.

Pan, B., Burbank, D.W., Wang, Y., Wu, G., Li, J., Guan, Q., 2003. A 900 k.y. record of strath terrace formation during glacial–interglacial transition in northwest China. Geology 31, 957–960.

Phillips, W.M., Sloan, V.F., Shroder Jr., J.F., Sharma, P., Clarke, M.L., Rendell, H.M., 2000. Asynchronous glaciation at Nanga Parbat, northwestern Himalaya Mountains, Pakistan. Geology 28, 431–434.

Potter Jr., N., Steig, E.J., Clark, D.H., Speece, M.A., Clark, G.M., Updike, A.B., 1998. Galena Creek rock glacier revisited — new observations on an old controversy. Geografiska Annaler 80A, 277–286.

Pratt, B., Burbank, D.W., Heimsath, A., 2002. Impulsive alluviation during early Holocene strengthened monsoons, central Nepal Himalaya. Geology 30, 911–914.

Pratt-Sitaula, B., Burbank, D.W., Heimsath, A.M., 2003. Significant advance during Younger Dryas, Annapurna region, Nepal. EOS-supplement. Transactions of the American Geophysical Union Fall Meeting 84 (46), F348.

Pratt-Sitaula, B., Burbank, D.W., Heimsath, A., Ojha, T., 2004. Landscape disequilibrium on 1,000 to 10,000 year scales Marsyandi River, Nepal, central Himalaya. Geomorphology 58, 223–241.

Putkonen, J., Swanson, T., 2003. Accuracy of cosmogenic ages for moraines. Quaternary Research 59, 255–261.

Rapp, A., 1960. Recent development of mountain slopes in Karkevagge and surroundings, Northern Scandinavia. Geografiska Annaler 42A, 65–200.

Schmidt, K.M., Montgomery, D.R., 1995. Limits to relief. Science 270, 617–620.

Shroder, J.F., Schreppy, R.A., Bishop, M.P., 1999. Denudation of small alpine basins, Nanga Parbat Himalaya, Pakistan. Arctic and Alpine Research 31, 121–127.

Shroder, J.F., Bishop, M.P., 2000. Unroofing of the Nanga Parbat Himalaya. In: Khan, M.A., Treloar, P.J., Searle, M.P., Jan, M.Q. (Eds.), Geological Society of London. Special Publication, vol. 170, pp. 180–200.

Sloan, V.F., Phillips, W.M., 1998. Asynchronous maximum advances of mountain glaciers in the Pakistan Himalaya. Geological Society of America, Abstracts with Programs 30, A–229.

Small, R.J., 1987a. Englacial and supraglacial sediment: transport and deposition. In: Gurnell, A.M., Clark, M.J. (Eds.), Glacio–Fluvial Sediment Transfer: an Alpine Perspective. Wiley Interscience, pp. 111–147.

Small, R.J., 1987b. Moraine sediment budgets. In: Gurnell, A.M., Clark, M.J. (Eds.), Glacio-Fluvial Sediment Transfer: an Alpine Perspective. Wiley Interscience, pp. 165–199.

Small, E.E., Anderson, R.S., 1998. Pleistocene relief production in Laramide mountain ranges, western United States. Geology 26, 123–126.

Small, E.E., Anderson, R.S., Repka, J.L., Finkel, R., 1997. Erosion rates of alpine bedrock summit surfaces deduced from in situ ^{10}Be and ^{26}Al. Earth and Planetary Science Letters 150, 413–425.

Stone, J.O., 2000. Air pressure and cosmogenic isotope production. Journal of Geophysical Research 105 (B10), 23,753–23,759.

Summerfield, M.A., Hulton, N.J., 1994. Natural controls of fluvial denudation rates in major world drainage basins. Journal of Geophysical Research 99 (B7), 13871–13883.

Summerfield, M.A., Stuart, F.M., Cockburn, H.A.P., Sugden, D.E., Denton, G.H., Dunai, T., Marchant, D.R., 1999. Long-term rates of denudation in the Dry Valleys, Transantarctic Mountains, southern Victoria Land, Antarctica based on in situ-produced cosmogenic ^{21}He. Geomorphology 27, 113–129.

Vance, D., Bickle, M., Ivy-Ochs, S., Kubik, P.W., 2003. Erosion and exhumation in the Himalaya from cosmogenic isotope inventories of river sediments. Earth and Planetary Science Letters 206, 273–288.

Wahrhaftig, C., Cox, A., 1959. Rock glaciers in the Alaska Range. Geological Society of America Bulletin 70, 383–436.

Walder, J.S., Hallet, B., 1986. The physical basis of frost weathering — toward a more fundamental and unified perspective. Arctic and Alpine Research 18, 27–32.

Whalley, W.B., 1984. Rockfalls. In: Brunsden, D., Prior, D.B. (Eds.), Slope Instability. Wiley, Chichester, pp. 217–256.

Whipple, K.X., Tucker, G.E., 1999. Dynamics of the stream-power river incision model: implications for heights of mountain ranges, landscape response timescales, and research needs. Journal of Geophysical Research 104 (B8), 17661–17674.

Whipple, K.X., Kirby, E., Brocklehurst, S.H., 1999. Geomorphic limits to climate-induced increases in topographic relief. Nature 401, 39–43.

Wobus, C., Heimsath, A., Whipple, K., Hodges, K., 2005. Active out-of-sequence thrust faulting in the central Nepalese Himalaya. Nature 434, 1008–1011.

Zeitler, P.K., Meltzer, A.S., Koons, P.O., Craw, D., Hallet, B., Chamberlain, C.P., Kidd, W.S., Park, S.K., Seeber, L., Bishop, M.P., Shroder, J.F., 2001. Erosion, Himalayan geodynamics, and the geomorphology of metamorphism. GSA Today 11, 4–8.

Zhang, P., Molnar, P., Downs, W.R., 2001. Increased sedimentation rates and grain sizes 2–4 Myr ago due to the influence of climate change on erosion rates. Nature 410, 891–897.